Multipoint observations of dipolarization front formation by magnetotail reconnection

A. Runov,[1] V. Angelopoulos,[1] and X.-Z. Zhou[1]

Received 10 November 2011; revised 16 March 2012; accepted 13 April 2012; published 25 May 2012.

[1] We present multipoint observations of magnetotail plasma sheet dynamics during an event in which magnetic reconnection and dipolarization were observed at $-16 < X < -15$ R_E (mid-tail) and at $-10 < X < -4.8$ R_E (near-Earth plasma sheet), respectively. Timing analysis of the observations shows that the near-Earth dipolarization was a consequence of mid-tail reconnection. Large-amplitude magnetic field oscillations were observed in the temporal and spatial vicinity of the reconnection site. Interpreted as current sheet flapping, they enable reconstruction of a complex sheet structure with an embedded thin current sheet of ion inertial scale size. Detailed analysis of the orientation of the dipolarization front and of plasma motions around it reveals that the front of the reconnection jet was interchange unstable.

Citation: Runov, A., V. Angelopoulos, and X.-Z. Zhou (2012), Multipoint observations of dipolarization front formation by magnetotail reconnection, *J. Geophys. Res.*, *117*, A05230, doi:10.1029/2011JA017361.

1. Introduction

[2] Magnetic reconnection is widely recognized as the key process in the conversion of magnetic energy to plasma kinetic and thermal energies in the magnetosphere [e.g., *Vasyliunas*, 1975; *Birn and Priest*, 2007]. Reconnection in the magnetotail is the most plausible cause of burst-like transport of mass, flux, and energy in the magnetotail plasma sheet via bursty-bulk flows (BBFs) [*Angelopoulos et al.*, 1992, 1994] and rapid flux transport events(RFT) [*Schödel et al.*, 2001a, 2001b] leading to high-energy particle injections into inner magnetosphere [e.g., *Birn et al.*, 1997a, 1997b]. Although according to statistics, the reconnection region is located at $-30 < X < -20$ R_E [*Nagai et al.*, 1998; *Eastwood et al.*, 2010], its actual location depends on magnetic activity [e.g., *Nagai et al.*, 2005]. Signatures of reconnection have been observed as close to the Earth as $X \approx -14$ R_E [*Sergeev et al.*, 2008]. Despite several decades of observations and intense theoretical studies, the mechanism of magnetotail reconnection onset and details of particle energization during reconnection are largely unknown and debatable [e.g., *Sitnov and Swisdak*, 2011].

[3] The classical observable signatures of magnetotail reconnection are corresponding magnetic field and bulk velocity reversals detected by spacecraft monitoring the plasma sheet (see, e.g., *Birn and Priest* [2007] and *Eastwood et al.* [2010] for reviews). To observe these signatures, spacecraft should be in the central plasma sheet. Although those located away from the neutral sheet vicinity might easily miss classical flow field reversal, they could observe remote (non-classical) signatures of reconnection, such as plasma inflow and characteristic features in particle distribution functions. These non-classical observable signatures were described and successfully utilized in recent multiprobe studies [*Zhou et al.*, 2009; *Angelopoulos et al.*, 2009].

[4] Although physical mechanisms of magnetotail reconnection onset are debatable, formation of a thin current sheet (TCS) with a half-thickness of an ion inertial length ($d_i = c/\omega_{pi}$, where ω_{pi} is the ion plasma frequency) has been established as a necessary condition for reconnection onset (see *Schindler* [2007] and *Baumjohann et al.* [2007] for reviews). Thin current sheets were indeed observed *in situ* prior to or at flow reversals in the magnetotail at a radial distance of 19 R_E [*Nakamura et al.*, 2006; *Runov et al.*, 2008a]. The TCSs are embedded in a thicker plasma sheet, and their structure is quite different from the Harris solution, which is commonly used for modeling of current sheet dynamics [see, e.g., *Petrukovich et al.*, 2011, and references therein]. The radial lengths and cross-tail widths of TCSs are as yet unknown. It is also important to resolve TCS structure, including profiles of magnetic field gradient and plasma density, to understand the type of plasma instability responsible for reconnection onset.

[5] Dipolarization fronts, rapid (1–10 s) large-amplitude (few tens of nT) increases in the north-south magnetic field component (B_z) [*Runov et al.*, 2009], are often observed at the leading edge of BBFs in the plasma sheet at X from -30 to -7 R_E [*Ohtani et al.*, 2004]. Their thickness is typically comparable with the thermal ion gyroradius [*Runov et al.*, 2011]. Earlier two-point observations [*Russell and McPherron*, 1973; *Moore et al.*, 1981; *Ohtani*, 1998], and recent observations by

[1]Department of Earth and Space Sciences, UCLA, Los Angeles, California, USA.

Corresponding author: A. Runov, Department of Earth and Space Sciences, UCLA, 3845 Slichter Hall, Los Angeles, CA 90095, USA. (arunov@igpp.ucla.edu)

0148-0227/12/2011JA017361

Cluster [*R. Nakamura et al.*, 2002] and THEMIS [*Runov et al.*, 2009; *Sergeev et al.*, 2009] have provided strong evidence of Earthward propagation of the dipolarization fronts. Comprehensive analysis of THEMIS observations has also shown that dipolarization fronts are boundaries between the ambient plasma sheet and intruded energetic plasma populations [*Runov et al.*, 2011].

[6] Since dipolarization fronts are often observed along with fast plasma flows, it seems natural to consider them as remote consequences of magnetic reconnection in the magnetotail. And, indeed, dipolarization front formation has been demonstrated in various types of simulations of reconnection. Although, typically, a front thickness is comparable to an ion gyroradius requiring a kinetic description, MHD simulations also reproduce some larger-scale front features [*Wiltberger et al.*, 2000; *Ge et al.*, 2011; *Birn et al.*, 2011]. Formation of dipolarization fronts has been also reported in hybrid simulations [*Hesse et al.*, 1998; *Krauss-Varban and Karimabadi*, 2003]. Hybrid models have reproduced key front plasma signatures: flow increase ahead of the front [*Hesse et al.*, 1998; *Zhou et al.*, 2011] and higher-speed flow away from the neutral sheet [*Krauss-Varban and Karimabadi*, 2003]. Particle-in-cell (PIC) simulations have demonstrated formation of a dipolarization front within $\sim 10\ c/\omega_{pi}$ of the initial X-line [*Sitnov et al.*, 2009; *Pritchett*, 2010]. The transient character of electric field (in the spacecraft frame) enhancement at dipolarization fronts with a typical of 40 s - 1 min [*Runov et al.*, 2011], suggests impulsive reconnection in the magnetotail plasma sheet [*Semenov et al.*, 1992] as its source.

[7] Three-dimensional hybrid simulations have shown that a reconnection jet of finite cross-tail width is interchange unstable [*M. S. Nakamura et al.*, 2002]. This instability leads to azimuthal structuring of the jet's leading edge and the dipolarization front, which is the interphase between reconnected and ambient plasmas. Interchange or ballooning-type instabilities may develop in the magnetotail plasma sheet with a local minimum in B_z [see *Pritchett and Coroniti*, 2010, and references therein]. Such a configuration, resulting from local current sheet thinning, has been observed [*Sergeev et al.*, 1994; *Saito et al.*, 2010]. Some evidence of ballooning instability prior to reconnection has recently been found in global MHD simulations [*Raeder et al.*, 2010]. MHD and PIC simulations have also demonstrated dipolarization front formation due to steepening of the interchange-unstable initial tailward B_z gradient [*Pritchett and Coroniti*, 2010; *Guzdar et al.*, 2010; *Pritchett and Coroniti*, 2011]. The current sheet with a local B_z minimum may also be kink- [*Pritchett et al.*, 1996; *Erkaev et al.*, 2008, 2009] and tearing-[*Sitnov and Schindler*, 2010] unstable. Moreover, 3-D PIC simulations of the interchange instability in a region of tailward equatorial magnetic field gradient have shown that reconnection develops in the tailward wake of an "interchange finger head" [*Pritchett and Coroniti*, 2011]. In the simulations, reconnection occurs about 20–30 characteristic proton gyroperiods later than dipolarization front formation due to interchange instability. Two-dimensional PIC simulations with open boundary conditions also have showed secondary X-line formation behind the dipolarization front [*Sitnov and Swisdak*, 2011].

[8] Thus, the relationship between magnetotail reconnection and dipolarization front formation could be very complex, including a variety of processes associated with TCS formation and dynamics in the plasma sheet. To observe these dynamics *in situ*, a fleet of spacecraft that can make simultaneous observations in the mid-tail ($-40 < X < -10\ R_E$) and near-Earth (earthward of $X \approx -10\ R_E$) plasma sheet regions is needed. The space segment of the THEMIS mission [*Angelopoulos*, 2008; *Sibeck and Angelopoulos*, 2008] was able to monitor these plasma sheet regions during magnetotail conjunction events. THEMIS spacecraft cross-tail separations during the conjunction intervals, however, were not sufficiently numerous to study the effects of interchange instability. To compensate for the lack of azimuthal sampling, intervals of THEMIS conjunctions supplemented by geosynchronous satellites are especially useful.

[9] In this study we analyze magnetotail observations by THEMIS and two GOES spacecraft during an event at which reconnection and dipolarization front signatures were detected in the mid-tail and near-Earth plasma sheet, respectively, with the main goal of understanding the physical relationship between processes observed in those regions. In section 2 we examine observations in the two plasma sheet regions and the time delays between them. Possible scenarios of plasma sheet dynamics supported by these observations are discussed in section 3. Even though a single event is comprehensively presented here, we briefly overview similar events in section 4.

2. Data Analysis

2.1. Event Description

[10] The entire day of 1 March 2008 was geomagnetically active; the K_p index varied between 3 and 5+. A set of substorms and activations observed by THEMIS ground-based observatories and spacecraft was studied and modeled [*Runov et al.*, 2008b; *El-Alaoui et al.*, 2009; *Ashour-Abdalla et al.*, 2009]. In this paper, we will discuss THEMIS plasma sheet observations between 0200 and 0230 UT. The solar wind and IMF parameters as well as ground-based magnetic data for this interval are summarized in *El-Alaoui et al.* [2009]. According to standard T96-based mapping [*Tsyganenko*, 1995], the inner THEMIS probes foot points were in the field of view of the KUUJ and SNKQ stations. Corresponding all-sky images are available on-line at http://themis.ssl.berkeley.edu/.

[11] Each THEMIS spacecraft (probe) carries identical instrumentation [*Angelopoulos*, 2008]. The Fluxgate Magnetometer (FGM) [*Auster et al.*, 2008] provides DC magnetic field measurements with a temporal resolution of 128 vectors per second during the burst mode. The Search Coil Magnetometer (SCM) measures low-frequency magnetic field fluctuations and waves in three directions within the 0.1 Hz to 4 kHz frequency band [*Roux et al.*, 2008]. The Electric Field Instrument (EFI) [*Bonnell et al.*, 2008] measures electric field with a 0.125 Hz sample rate. The electric (EFI) and magnetic (SCM) field spectral products (Filter Bank Data, FBK) are computed on-board by the Digital Fields Board (DFB) [*Cully et al.*, 2008]. The Electrostatic Analyzer (ESA) [*McFadden et al.*, 2008] provides ion and electron distribution functions in the 5 eV to 25 keV energy range with a time resolution of 1 3-D distribution function per spin in the burst mode. The Solid State Telescope (SST) [*Angelopoulos*, 2008] detects high-energy (30 keV - 1 MeV) ion and electron fluxes with a time-resolution of 1 3-D distribution function per spin in the burst mode.

[12] Figure 1 shows THEMIS probe locations, magnetic field, and bulk velocity observed by probes P1-P4. The

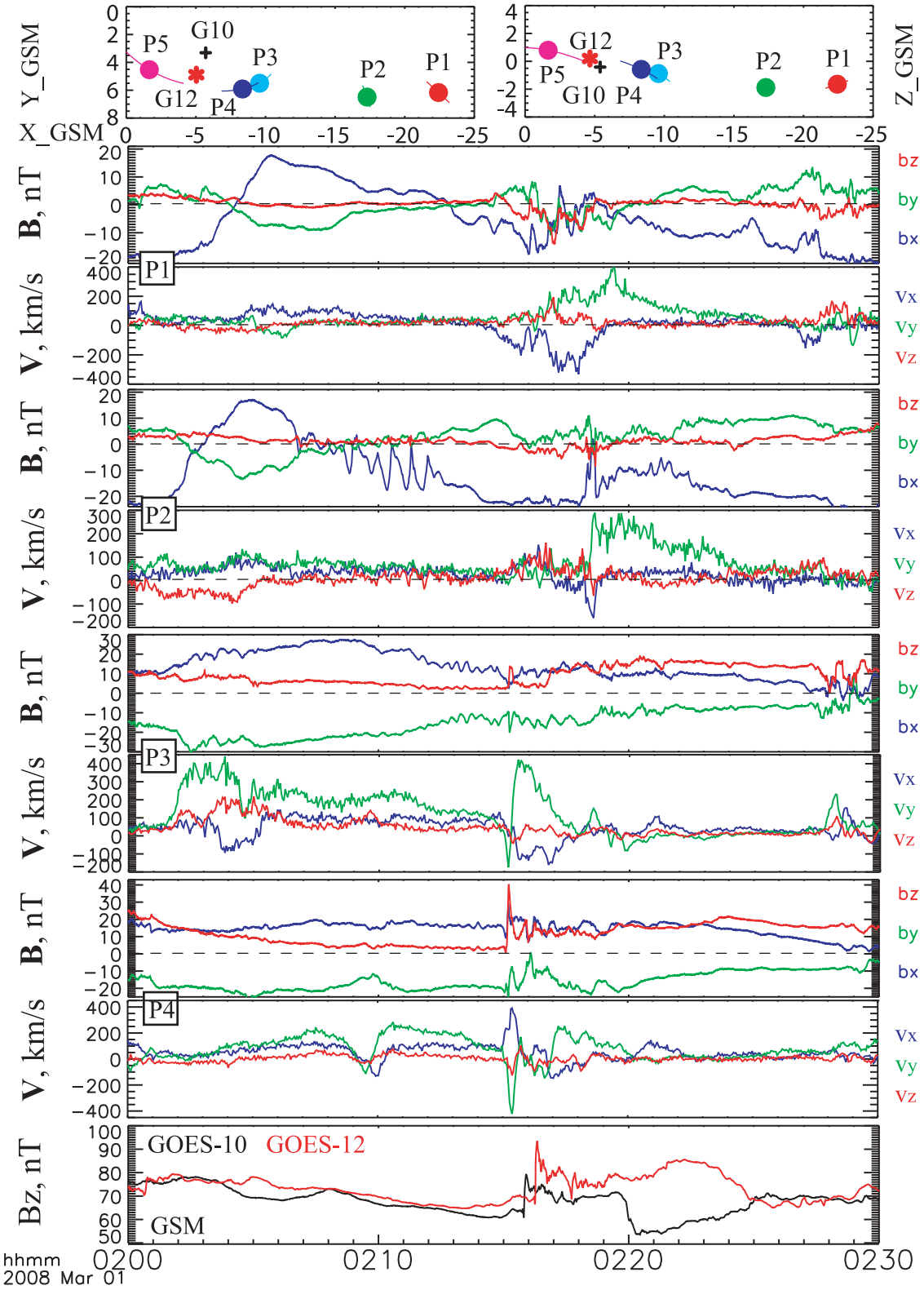

Figure 1. THEMIS, GOES-10, and GOES-12 positions in *XY* and *XZ* GSM planes; magnetic field and bulk velocity time series at P1, P2, P3, and P4; B_z (GSM) at GOES-10 and GOES-12 between 0200 and 0230 UT on March 1, 2008.

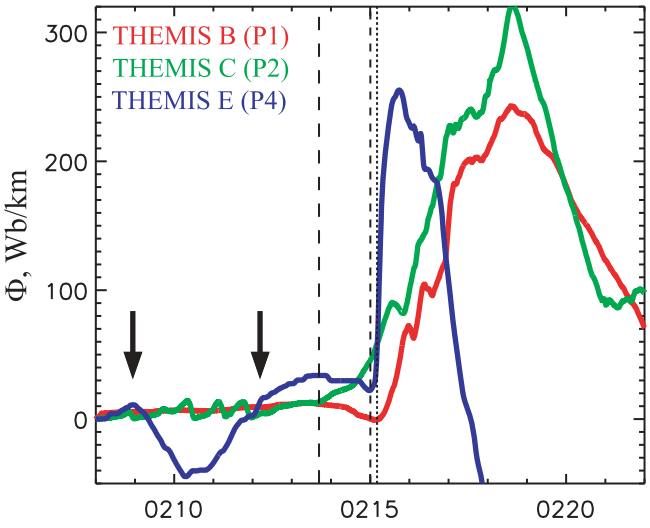

Figure 2. Cumulative flux transfer $\Phi = -\int_0^\tau E_y dt$ at P1 (red), P2 (green), and P4 (blue) between 0208 and 0232 UT. Dotted, short-dashed, and long-dashed lines indicate onset of flux transfer at P2, P4, and P1, respectively. Arrows indicate interval of current sheet flapping at P2.

THEMIS fleet was in major conjunction i.e., tail-elongated, with the most distant probe (P1) located at [−22.4, 6.2, −1.6] R_E (GSM), P2 at [−17.3, 6.5, −1.9] R_E, and a pair of near-Earth probes (P3 and P4) at [−9.6, 5.5, −0.8] and [−8.4, 5.9, −0.6] R_E, respectively. Two geostationary satellites GOES-10 and GOES-12 were in good conjunction with the THEMIS fleet situated at [−5.8, 3.2, −0.1] and [−4.8, 4.6, −0.1] R_E, respectively. This configuration provides an excellent opportunity to study disturbance propagation in the magnetotail.

[13] At around 021 4:30 UT P1, situated in the southern half of the plasma sheet at $B_X \approx -10$ nT, detected tailward flow onset accompanied by a bipolar northward then southward variation in B_z. These observations may be interpreted as signatures of reconnection earthward of P1. The tailward flow velocity, calculated using input from both particle detectors (ESA and SST), reached approximately −300 km/s.

[14] Between 0209 and 0213 UT, P2 observed large-amplitude, quasiperiodic magnetic field oscillations with B_x varying from 0 to −20 nT. Later on, P2 detected an increase in $|B_x|$, which indicates plasma sheet thinning. Between 0214 and 0218 UT, P2 remained at $B_X \approx -25$ nT detecting plasma flow toward the neutral sheet ($V_Z \approx 100$ km/s). During a fast excursion into the vicinity of the neutral sheet between 0218 and 0219 UT, P2 detected tailward flow at $V_X \approx -200$ km/s with peaks in B_y and $B_z \approx 10$ and −5 nT, respectively. The flow rotated duskward later on. Most likely, missed the classical signatures of reconnection (i.e., fast flow and corresponding signatures in B_z). The northward ($V_z > 0$) plasma flow detected by P2 at $B_X \approx -20$ nT may be interpreted as inflow to the reconnection region. Since B_x did not change, the northward flow cannot be attributed to current sheet thinning.

[15] At about 0202 UT, P3 and P4, situated in the near-Earth plasma sheet, began to detect an increase in B_x (more pronounced at P3) with a simultaneous decrease in B_z (more visible in the P4 time series). Both probes also detected an increase in plasma velocity, mainly in the V_y-component. This velocity increase was due to duskward-drifting energetic ions. These observations indicate thinning and stretching of the current sheet [*Petrukovich et al.*, 2007; *Zhang et al.*, 2011]. Between 0215 and 0216 UT, P4 detected an abrupt increase in B_z up to 40 nT (at 0215:06 UT), preceded by a short dip to ∼0, and an approximately 1-min-long enhancement in the plasma bulk flow with peaks in V_x and in $V_y \approx 350$ and −350 km/s, respectively. The observed B_z signatures are typical of dipolarization fronts [e.g., *Runov et al.*, 2011]. P3 detected a much smaller-amplitude (peak of 14 nT) jump in B_z 6 s later (at 0215:12 UT) than P4. The front passed the both probes within ≈30 s and was followed by a gradual, smaller-amplitude dipolarization.

[16] A distinct dipolarization front with $\Delta B_z \approx 20 - 25$ nT was also detected by the two geostationary satellites, GOES-10 and GOES 12, at 0215:50 and at 0216:15, respectively. Immediately before front detection, GOES-10 and GOES-12 observed $B_x = 51$ and 29 nT, respectively (not shown; GOES magnetometer data are available at the THEMIS web site http://themis.ssl.berkeley.edu/). Thus, the spacecraft situated 1.4 R_E closer to midnight and at larger B_x detected the front earlier than that located duskward and closer to the magnetic equator.

[17] Auroral intensification onset was detected by SNKQ at 0215:09 UT. A new bright spot appeared on the east side of SNKQ's field of view at 0215:27 UT (see mosaic images at themis.ssl.berkeley.edu).

[18] Figure 2 shows cumulative magnetic flux transport $\Phi = \int E_y dt$ [*Liu et al.*, 2011] at P1, P2, and P4 from 0208 to 0222 UT. The earliest indication of rapid flux transport was detected by P2 at about 0213:40 UT (long-dashed vertical line). Comparison with the bulk velocity shown in Figure 1 indicates that the flux transfer at P2 was due to enhanced northward velocity (V_z) observed simultaneously with $B_X \approx -20$ nT. The northward velocity may be interpreted as inflow to the reconnection region, which was localized in the vicinity of the neutral sheet and missed by P2 because of its exit from the central plasma sheet. P4, situated 8.9 R_E earthward of P2, detected a jump in flux transport at 0215:06 UT (short-dashed line) when the dipolarization front hit the probe. P1, located 5.1 R_E tailward of P2, detected flux transfer onset at about 0215:10 UT (dotted line). A minimum in Φ at P4 between 0209 and 0212 UT (bounded by arrows) is associated with a short period of $V_X < 0$ while $B_Z > 0$ (see Figure 1). The flux transport behavior at P1 and P2 is similar to the integrated electric field time variations observed in the reconnection region in MHD simulations [*Birn et al.*, 2011].

2.2. P2 Observations Prior to Flux Transfer Onset

[19] Between 0208 and 0213 UT, immediately before flux transfer onset, P2 observed quasiperiodic oscillations in B_x with an amplitude of 15 nT and an average period of 60 s. Examination of P2 observations during the B_x oscillations shown in Figure 3 may provide important information on plasma and current sheet structure near reconnection onset. For convenience, each oscillation period is marked by a letter (A to F) with a sign (±) corresponding to the sign of $\partial B_x/\partial t$: plus and minus for increasing and decreasing B_x, respectively. Comparison of Figures 3a and 3b shows that

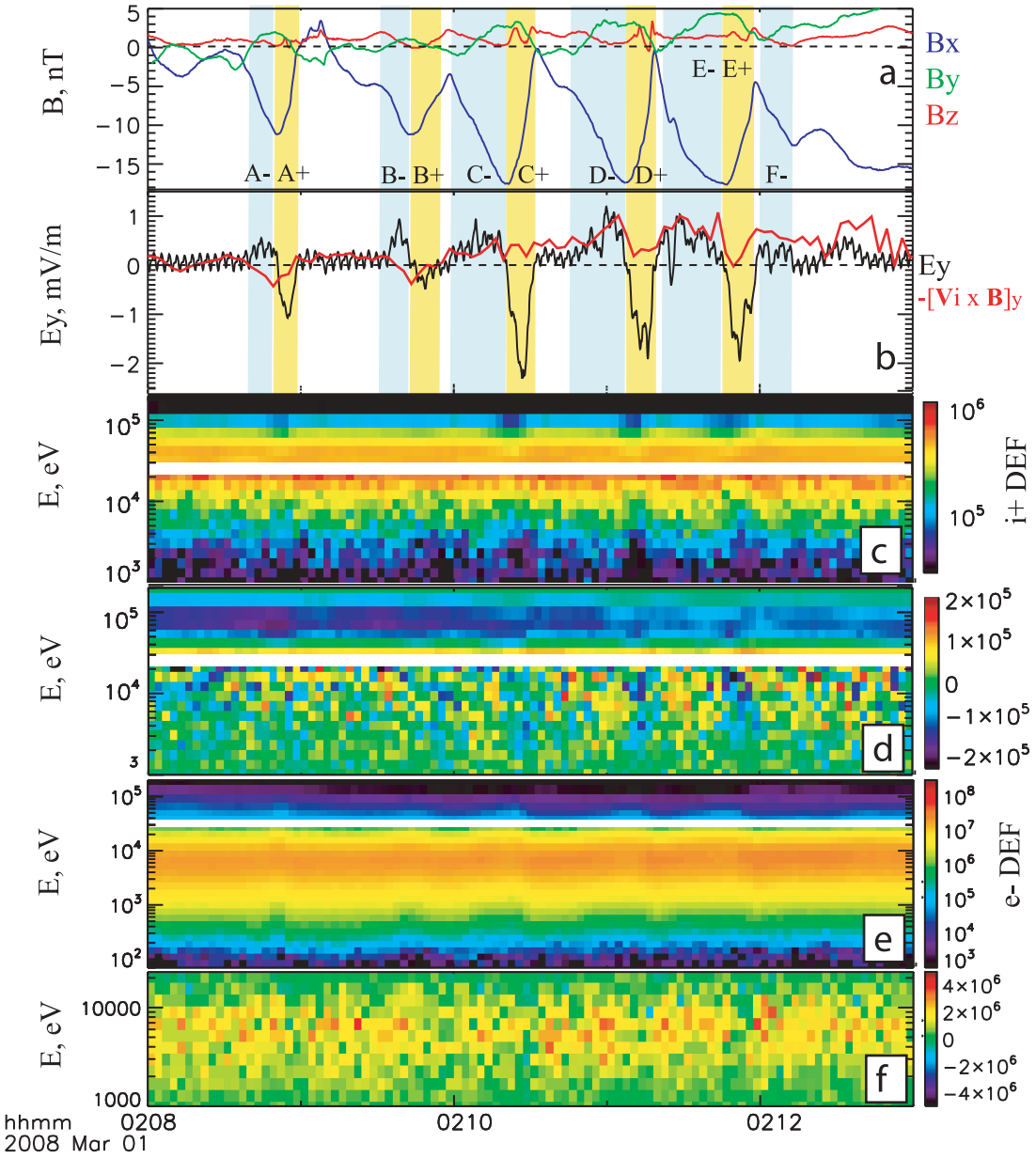

Figure 3. Summary plot of THEMIS C (P2) observations during current sheet flapping between 0208 and 0213 UT: (a) magnetic field GSM components; (b) -Ey (DSL) from EFI and $-[\mathbf{V}_i \times \mathbf{B}]_y$; (c) ion and (e) electron energy-time spectrogram, differential flux (DEF, eV/s/cm^2/eV) is color coded; difference between (d) ion and (f) electron energy flux in $-45° > \theta > -90°$ and $90° > \theta > 45°$ bins.

negative $\partial B_x/\partial t$ intervals (blue bars) correspond to positive E_y, observed by EFI, whereas positive $\partial B_x/\partial t$ intervals (yellow bars) correspond to negative E_y. The EFI measurements are in reasonable agreement with $-\mathbf{V}_i \times \mathbf{B}$ during intervals B+, C−, D−, E− and F−. However, during intervals of rapid B_x changes (A−, A+, C+, D+, and E+), EFI E_y disagrees with $-[\mathbf{V}_i \times \mathbf{B}]_y$. A reason for this disagreement is, most likely, instrumental: when the significant part of the ion population is within the SST energy range ($E > 30$ keV), the thermal plasma velocity (1000 km/s) is so large that thermal noise prohibits accurate measurement of the vertical plasma velocity. However, E_y and $[\mathbf{V}_i \times \mathbf{B}]_y$ disagreement may also be due to decoupling of ion and electron motion. The spectrogram in Figure 3d shows dropouts in the high-energy ion flux and decreases in the low-energy flux during intervals with positive $\partial B_x/\partial t$ (yellow bars). Conversely, the high-energy electron flux increased during "plus" and decreased during "minus" intervals (f). The average electron energy increased gradually during the entire interval. The difference between northward and southward ion and electron fluxes at energies below ~20 keV became (on average) positive and negative during "minus" and "plus" half-cycles, respectively (Figures 3e and 3g).

[20] Minimum variance analysis (MVA) [*Sonnerup and Scheible*, 1998] of the magnetic field during the entire B_x-oscillation interval (0208–0213 UT) yielded eigennumbers λ = [34.7, 0.81, 0.27]. The MVA eigennumbers represent actual field component variation (in nT^2) in the

Table 1. Magnetic Field Minimum Variance Analysis Results for P2 Flapping Current Sheet Crossings[a]

ID	UT (hhmm:ss)	MVA λ, nT^2	MVA **N**
A−	0208:35–0208:50	12.7, 0.32, 0.02	0.07, −0.03, 0.99
A+	0208:50–0208:59	14.1, 0.15, 0.08	0.15, −0.80, 0.57
B−	0209:30–0209:45	6.52, 0.062, 0.009	0.29, −0.17, 0.94
B+	0209:45–0209:57	4.08, 0.023, 0.004	0.15, −0.99, 0.02
C−	0209:58–0210:19	18.6, 0.094, 0.006	−0.12, 0.05, 0.99
C+	0210:19–0210:31	23.5, 0.64, 0.02,	0.22, −0.91, 0.35
D−	0210:31–0211:08	26.9, 0.46, 0.06	−0.08, 0.04, 0.99
D+	0211:08–0211:19	24.7, 0.93, 0.02	0.25, −0.94, 0.21
E−	0211:20–0211:47	24.3, 0.14, 0.02	−0.09, −0.24, 0.96
E+	0211:47–0211:59	14.9, 0.25, 0.001	0.25, −0.86, 0.44
F−	0212:00–0212:14	4.86, 0.068, 0.004	0.11, 0.28, 0.95

[a]The MVA normal vector **N** components are shown in the GSM coordinate system.

corresponding directions. If the medium-to-minimal eigenvalue ratio $r_{23} = \lambda_2/\lambda_3$ is sufficiently large (factor of 5–10), the minimum variance direction, which corresponds to the smallest eigennumber (λ_3), may be interpreted as normal to the tilted current sheet [*Sonnerup and Scheible*, 1998; *Sergeev et al.*, 2006]. The obtained minimum variance direction **N** = [−0.14, −0.44, 0.88] indicates a significant current sheet tilt in the $(YZ)_{GSM}$ plane. MVA results for each of half-cycle from A− to F− are summarized in Table 1. Analysis revealed MVA minimum variance direction rotation in the $(YZ)_{GSM}$ plane: N_y is small (positive or negative) for "minus" intervals and large negative for "plus" intervals. Since r_{23} >10 for most intervals, the corresponding eigenvector **N** may be interpreted as the current sheet normal direction. Figure 4 shows projections of the MVA-based current sheet normals during "plus" (red circles) and "minus" (blue circles) crossings. An asterisk corresponds to the normal resulting from MVA application for the entire flapping interval, which provides a "zero" tilt direction (dashed line). All projections are close to a unit circle, indicating normal rotation in the *YZ* plane. Such rotation is the most distinctive feature of current sheet flapping [*Sergeev et al.*, 2004, 2006; *Runov et al.*, 2005a].

[21] Current sheet flapping, during which a probe tracks a large portion of the current sheet, makes it possible to study current sheet structure [*Sergeev et al.*, 1998; *Runov et al.*, 2005b, 2006]. In our case, P2 scanned the southern half of the current sheet from $B_X \sim 0$ to, on average, $B_X \approx -15$ nT. The spectrograms in Figure 3 indicate that magnetic field variations were associated with vertical motion of low-energy ions and electrons. Therefore, integration of vertical (V_z) convection velocity allows us to estimate scale and magnetic field gradient in the flapping current sheet [*Sergeev et al.*, 1998, 2003]. As mentioned above, ion V_z is not reliable. Because the plasma sheet was hot (see spectrograms in Figure 3), the second moment of the electron distribution functions cannot be used for V_z calculation either (the electron thermal velocity was 15×10^3–20×10^3 km/s, which makes recovery of the electron bulk velocity from a distribution function shift impossible). Assuming that the observed variations in E_y (Figure 3b) are due to magnetic flux transport during current sheet motion in the north-south direction with respect to the stationary spacecraft, the corresponding velocity has been estimated from electric and magnetic field measurements as $V_{Dz} = E_y B_x / B^2$. Figure 5 shows the calculated vertical velocity and its integral over entire flapping time interval. The resulting path *S* may be interpreted as the flapping current sheet profile in the *YZ* plane: above the *S* curve $B_X > 0$ (earthward) and below the curve $B_x < 0$ (tailward). The red dashed line shows an estimate of the P2 path through the flapping current sheet; vertical dashed lines indicate times of P2 current sheet proximity. Although crude, the resulting profile provides flapping amplitude estimates of 1000 km (approximately the thermal gyroradius). Also notable is that the current sheet surface wave is far from quasi-sinusoidal. The profile exhibits a set of folds with much larger steepness during "plus" intervals, when the current sheet was almost vertical (with large negative N_y, see Table 1).

[22] Separate integration of V_{Dz} during each current sheet crossing provides a way to reconstruct vertical profiles of the magnetic field gradient, which is a proxy for current sheet density in the flapping current sheet [*Sergeev et al.*, 1998, 2003]. The method works better for rapid, "smooth" crossings with minimum temporal variation [*Runov et al.*, 2006]. Figure 6 shows $B_x(Z^*)$, $j_y(B_x)$, and $j_y(Z^*)$ profiles obtained

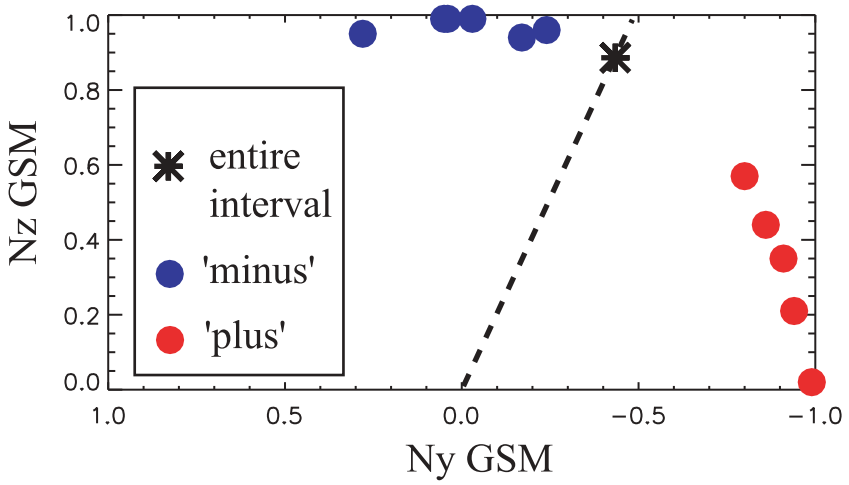

Figure 4. Projections of flapping current sheet MVA normal vectors onto the $\{N_y, N_z\}$ plane. A dashed line shows the projection of the normal, calculated for the entire flapping interval.

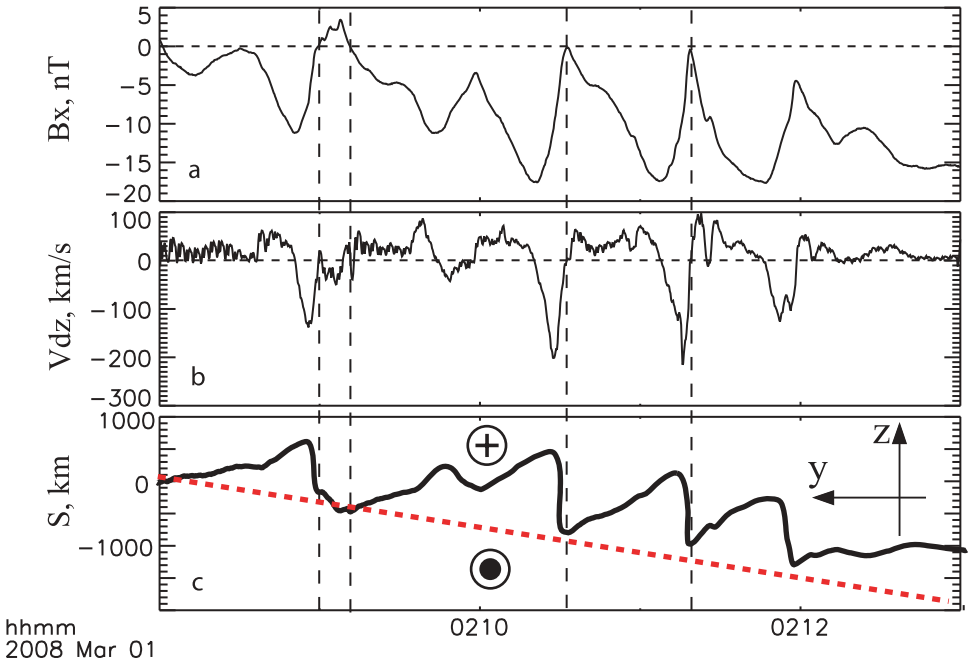

Figure 5. (a) B_x variations, (b) convection velocity $V_{Dz} = E_y B_x/B$, and (c) integrated vertical velocity $S = \int_{\tau_0}^{\tau_1} V_{Dz} dt$, where τ_0 and τ_1 are 0208:00 and 0213:00 UT, respectively. The dashed line shows approximated P2 trajectory.

during crossings A+, C+, and E+. $Z^* = \int_{\tau_s}^{\tau_f} V_{Dz} dt + Z_0$, where τ_s and τ_f are start and finish times for each crossing, respectively, is an effective vertical coordinate that is set to zero at minimum B_x. The profiles for the other crossings are appeared to be too noisy to recover any clear structure. The resulting scales should be treated with a caution: because the angle between the vertical velocity (V_{Dz}), which was used for the reconstruction, and current sheet normals during crossings A+, C+, and E+ was $\psi \approx 54$, 69, and 63°, respectively, the reconstructed scales may be significantly overestimated. The reconstruction gives upper estimates for the scales The lower estimates may be obtained as $Z^* \cos\psi$. Corresponding profiles of the electron density estimated from the measured spacecraft potential [e.g., *Mozer*, 1973] are shown in Figure 7. The j_y profiles exhibit similar characteristic features: 1) an increase in j_y profiles between $B_X = -10$ and -5 nT ($Z^* = -400$ and -200 km), indicating the presence of a thin current sheet (TCS) with scale (half-thickness) of ~100–200 km, embedded into thicker structure and 2) a local maximum at the current sheet periphery (at $B_X \approx -10$ nT and $Z^* \approx -600$ km for A+, $B_X \approx -16$ nT and $Z^* \approx -1000$ km for C+, $B_X \approx -16$ nT and $Z^* \approx -800$ km for E+). The reconstruction also suggests a fine "triple peak" structure of the embedded TCS. The number of samples, however, does not allow us to make a definitive statement on how real this structure is. Because of magnetic and electric field temporal variations, reconstructions of the current sheet structure during the other crossings did not reveal well-defined, repeating structures.

2.3. P3 and P4 and GOES 10 and 12 Observations of the Dipolarization Front

[23] Assuming that all four spacecraft observed the same structure, the time delay between THEMIS P3/P4 and GOES-10/12 dipolarization front detections indicates earthward propagation of the front. On the other hand, the time delay between P3 and P4 (−6 s) may indicate front nonplanarity or dawnward propagation. Figures 8a and 8b show projections of the MVA-based normals at P3, P4, GOES-10, and GOES-12 onto the *XY* and *XZ* GSM planes, respectively. The corresponding MVA eigenvalues and minimum variance vectors are summarized in Table 2.

[24] Figure 8c shows projections of plasma bulk velocity vectors onto the *XY* GSM plane. P3 first detected a short dawnward velocity rotation immediately ahead of the front, then dominantly duskward and tailward flow behind it. The drift velocity calculated from electric and magnetic fields exhibits similar behavior (not shown). P4, located 1.2 R_E earthward and 0.4 R_E duskward of P3, did not observe the duskward flow detected by P3. This may indicate vortex-like plasma motion behind the front.

[25] Detailed fields, electromagnetic waves, and particle observations at P3 and P4 within 2 min of front detection are shown in Figures 9 and 10, respectively. Within ≈3 s, both probes detected a sharp B_z increase (14 nT at P3 and 40 nT at P4) lasting 10–15 s. At P4, the B_z jump was preceded by a negative B_z dip of 2 nT amplitude. B_z returned to approximately undisturbed value (<5 nT) at P3, but stayed at 10–20 nT at P4. P4 detected strong *X* and *Y* electric field components lasting for about 20 s behind the front, whereas P3 detected a short electric field spike. Both probes observed strong broadband wave activity associated with electric field enhancement (Figures 9c and 9d and Figures 10c and 10d). At P4, the waves were mainly electrostatic and lasted at least one minute behind the front. P3 observed magnetic waves ahead of and at the front and a short enhancement in electric field waves immediately behind it. Ion ϕ-energy spectrograms (where ϕ is probe spin-phase angle with respect to the

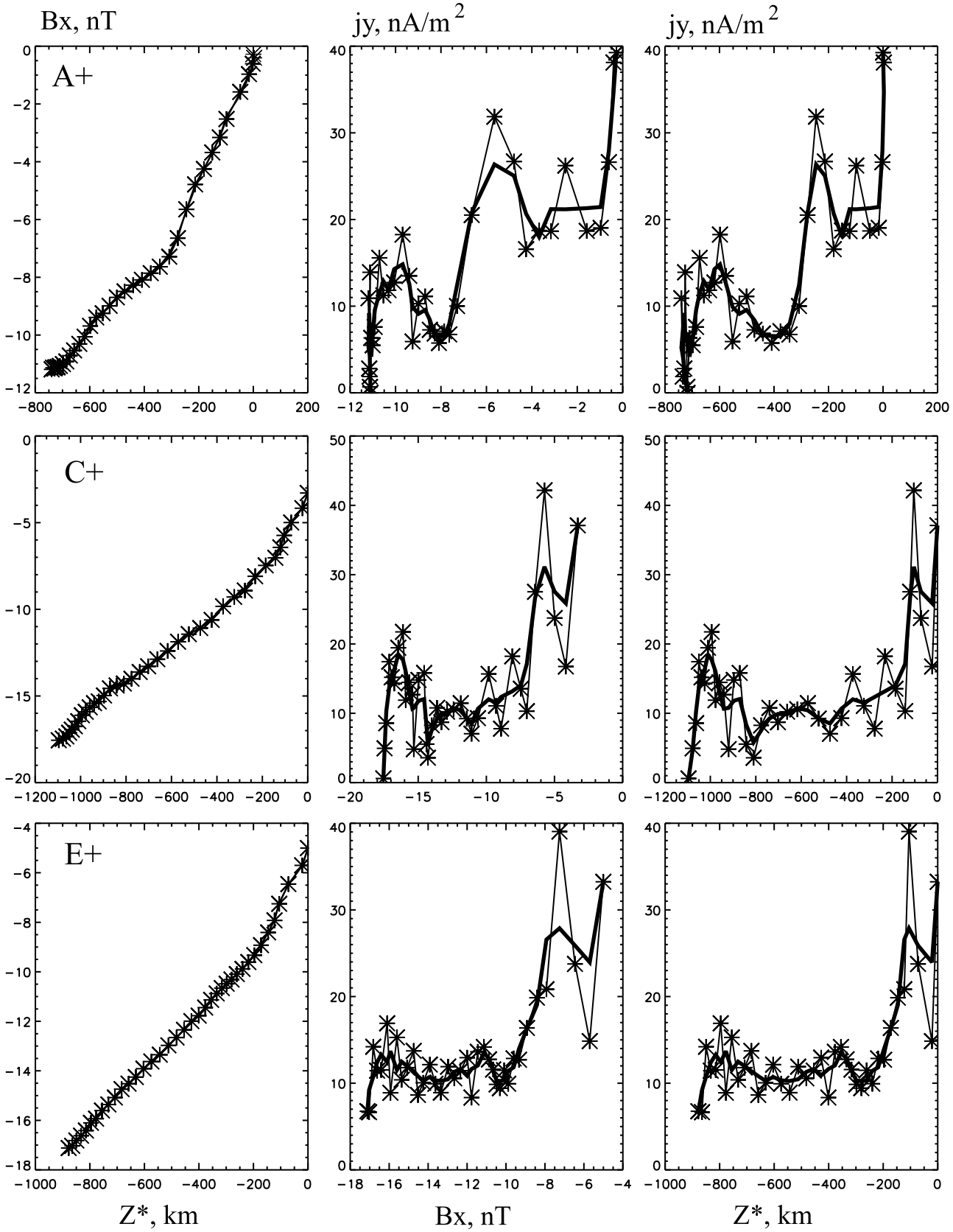

Figure 6. Crossings A+, C+ and E+: Profiles of (left) B_x and (right) $j_y \approx \mu_0^{-1}\Delta B_x/\Delta Z^*$ versus Z^*; (middle) j_y profile vs B_x. Thick lines are 3-point running averages of data (*).

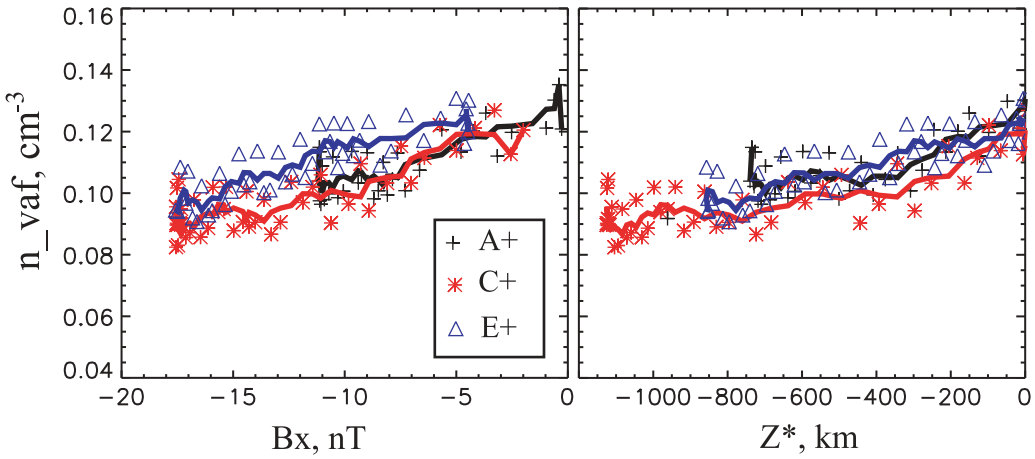

Figure 7. Profiles of electron density (n_{vaf}) estimated from the spacecraft potential observed during A+ (black), C+ (red) and E+ (blue) crossings. Solid lines are 3-point running averages of data.

sunward direction spectrograms, Figures 9e and 10e) at P4 demonstrate typical signatures observed at an earthward-moving dipolarization front: dropout in 1–10 keV ion energy flux at the front and appearance of a new, earthward-streaming ($\phi \approx 0°$) ion population at energies >10 keV, coexisting with ambient, duskward-drifting ions [*Zhou et al.*, 2010]. Ions are earthward-streaming behind the front at P4. P3 also detected 1–10 keV ion flux dropout at the front. The other signatures, however, differ from those at P4: the new population ahead of the front is more dawnward-moving (−90°), and the ions behind it are mainly duskward-drifting (90°). SST omni-directional energy-time spectrograms (Figures 9f and 10f) show an increase in electron fluxes at energies from ∼30 to ∼400 keV preceded by a short

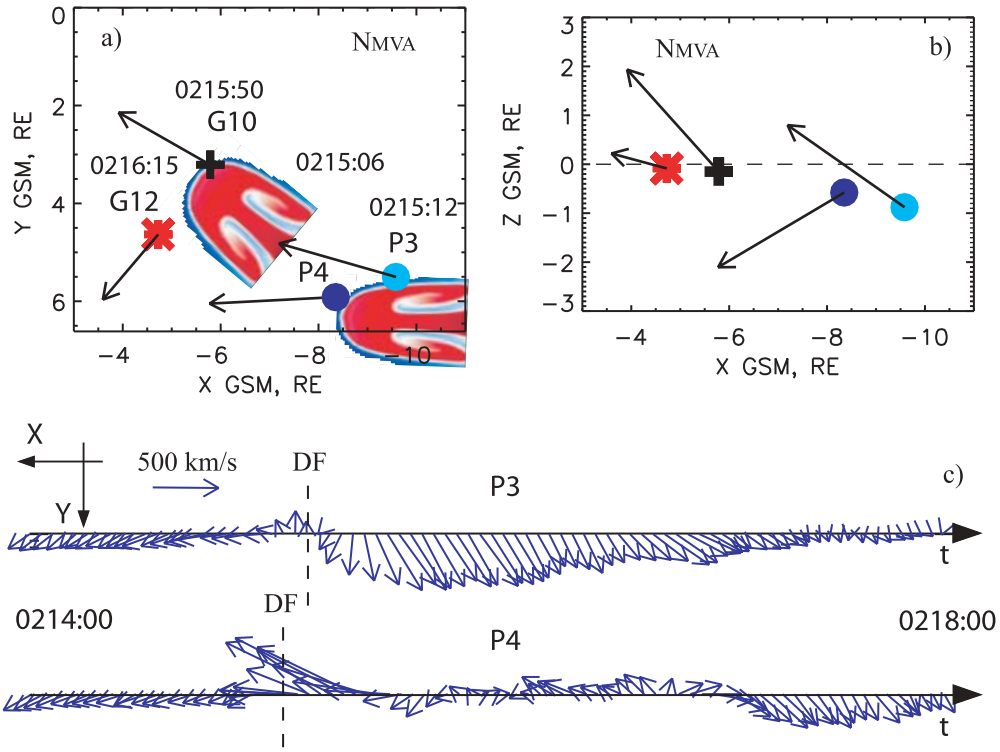

Figure 8. Projections of MVA-based dipolarization front normals (black arrows) at THEMIS P3, P4 and GOES 10 and 12 locations onto (a) $(XY)_{GSM}$ and (b) $(XZ)_{GSM}$ planes. A fragment of MHD simulation output from *Guzdar et al.* [2010], showing δB_z is used to illustrate a possible shape of the dipolarization front in Figure 8a. Note that simulated δB_z is out of scale (see text for details). (c) Time series of $(XY)_{GSM}$ projections of bulk velocity vector observed by P3 and P4 between 0214 and 0218 UT. Vertical dashed bars indicate dipolarization front (DF) arrival times.

Table 2. THEMIS P3 and P4, GOES-10, and GOES-12 Magnetic Field Minimum Variance Analysis Results

SC	UT (hhmm:ss)	MVA λ	MVA **N**
P3	0215:12–0215:15	27.8, 0.46, 0.08	0.79, −0.23, 0.56
P4	0215:07–0215:11.3	30.9, 1.6, 0.82	0.86, 0.04, −0.51
G10	0215:48–0215:56	69.9, 19.8, 1.08	0.62, −0.36, 0.69
G12	0216:14.5–0216:21	113.6, 5.72, 1.43,	0.38, 0.92, 0.12

decrease in 30–60 keV electron fluxes within ~20 s behind the front at both probes. Pitch angle distributions (PAD) of 0.2 – 30 keV electrons (Figures 9g and 10g) are quite different at P3 and P4, however. Those at P4 show two distinct electron populations: a relatively low-energy (~0.5 keV) isotropic ambient plasma sheet population ahead of the front and an energetic, largely anisotropic population behind it. PAD at energies >10 keV exhibit a pronounced triple-peak structure with maxima at 0, 180°, and 90°. At P3, the electron energy increases with front proximity and rapidly behind the front. PAD at energies >20 keV show enhancement in 90° electron flux. Those at energies between 1 and 20 keV exhibit a peculiar "bifurcating" structure with a peak at 90° immediately behind the front and a "two-hump" distribution with maxima around ±45°. Both probes detected a drop in plasma density behind the front. P4, however, observed a density increase ahead of the front, which is

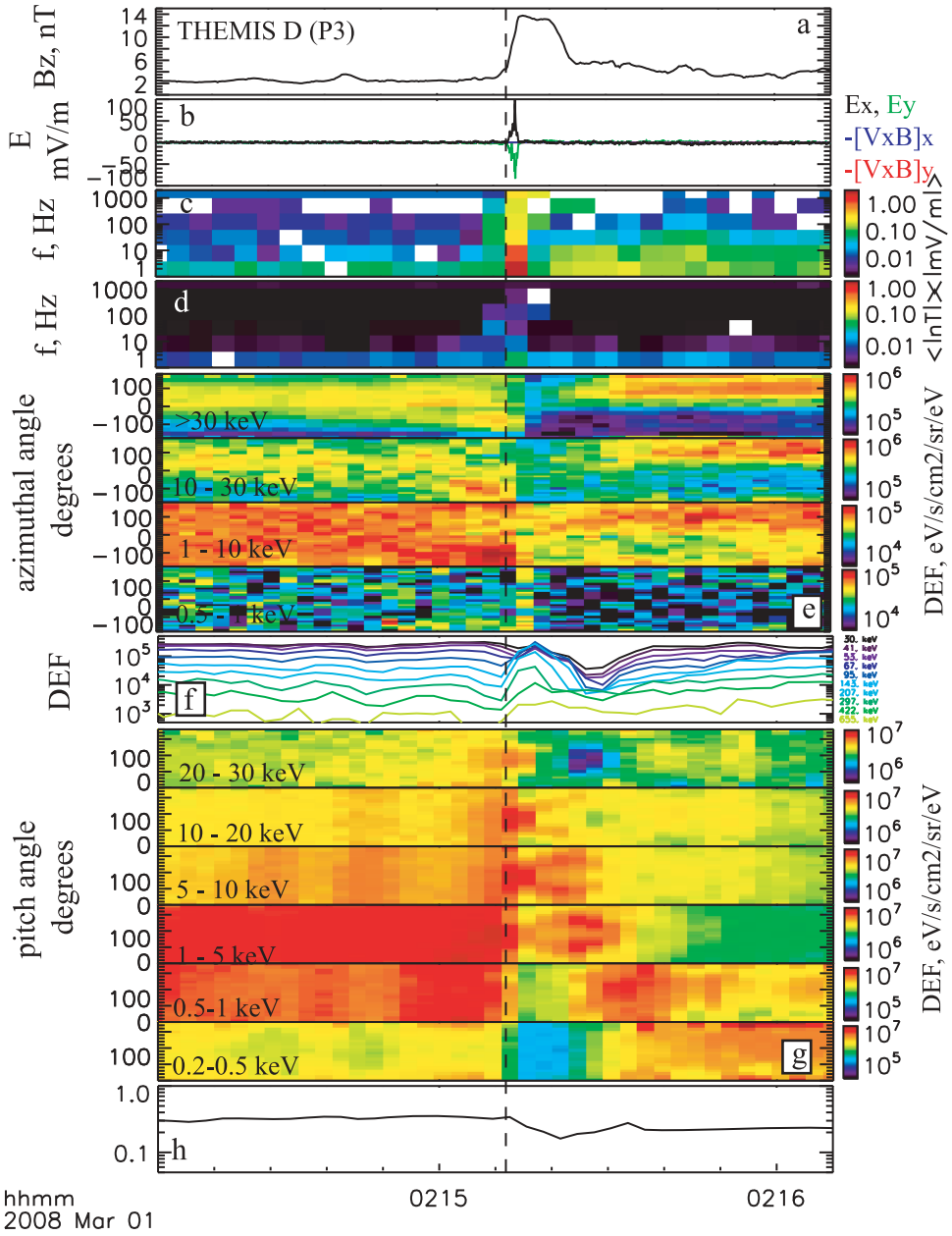

Figure 9. THEMIS D (P3) observations within 2 min of dipolarization front detection time (vertical dashed line). (a) GSM B_z; (b) E_x and E_y from EFI and corresponding $\mathbf{V} \times \mathbf{B}$; (c) electric and (d) magnetic wave power spectrograms from EFI and SCM filter bank, respectively; (e) ESA and SST ion Φ-energy spectrograms; (f) SST electron omni-directional spectrogram; (g) ESA electron PADs; (h) plasma density.

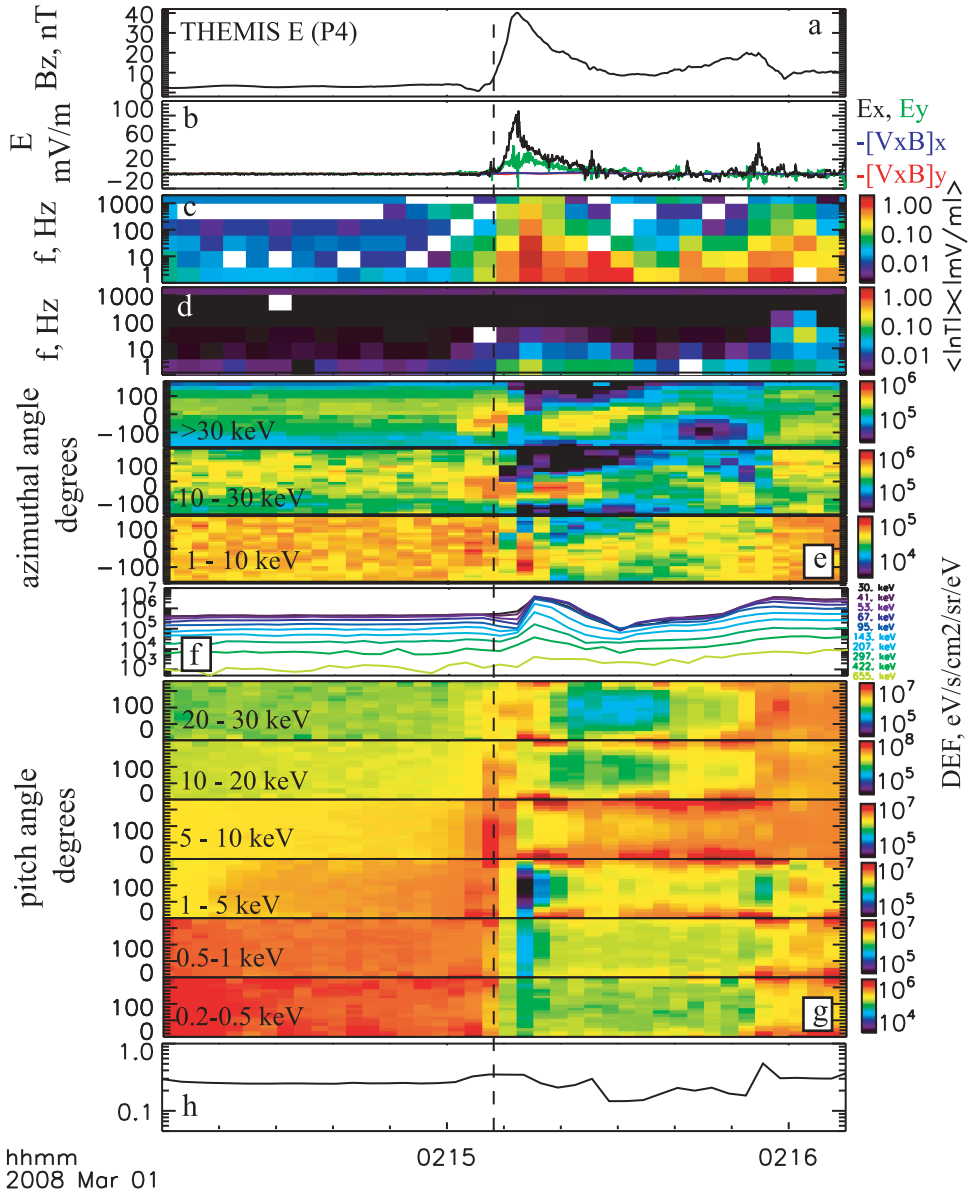

Figure 10. THEMIS E (P4) observations within 2 min of dipolarization front detection time (vertical dashed line) in the same format as Figure 9.

typical for earthward-moving dipolarization fronts [*Zhou et al.*, 2010; *Runov et al.*, 2011].

3. Discussion

[26] The above observations present evidence of plasma sheet reconnection earthward of $X \approx -22$ R_E, where tailward plasma flow carrying southward magnetic field was observed by the THEMIS P1, and signatures of an earthward-moving dipolarization front associated with vortical plasma motion were observed by two THEMIS probes (P3, P4) and two GOES satellites (GOES-10, GOES-12) at $-9.6 < X < -4.8$ R_E. Onsets of magnetic flux transfer were detected by P4 and P1 at $X = -8.4$ and at $X = -22.4$ R_E, respectively, with a time difference of 5 s, i.e., almost simultaneously. The probes were in conjunction with a separation in Y of 0.3 R_E. P1 detected tailward flow at $V_X \approx -300$ km/s, and P4 observed earthward flow at $V_X \approx 300$ km/s. It seems reasonable to assume that the tailward and earthward flows associated with southward and northward magnetic field, respectively, resulted from reconnection at approximately half the distance between P1 and P4, i.e., at $-16 < X < -15$ R_E, close to P2. Using the detected velocity of ± 300 km/s, the reconnection onset time may be estimated to be between 0212 and 0213 UT. Indeed, P2 at $X = -17.3$ R_E began to detect flux transport due to northward flow at $V_Z \approx 50 - 100$ km/s in the southern outer plasma sheet at 0213:40 UT. The timing is consistent with the an outflow velocity of 200–300 km/s. It is worth noting that B_z at P2 changed from small positive to negative at approximately 0214:30 UT. These B_z changes may be interpreted as signatures of the tailward-retreating X-line passing by the probe location.

[27] If, as assumed, reconnection occurred between 0212 and 0213 UT within 1–2 R_E of P2's location, flapping due to kinking or folding of the current sheet surface, observed by

P2 between 0208 and 0212 UT, may result from current sheet thinning prior to reconnection. MHD models of flapping show instability of a current sheet with a local B_z minimum ($\partial B_z/\partial x < 0$) [*Erkaev et al.*, 2008, 2009]. In the unstable region, the flapping perturbations increase but do not propagate. In adjacent regions, however, the current sheet may be stable, and flapping waves may propagate in the cross-tail direction. In our case, the rotation of current sheet normal in the *YZ* plane (Figure 4) indicates azimuthal propagation of the waves on the current sheet surface. Since only the southern half of the current sheet was crossed repeatedly, we cannot distinguish between current sheet kinking and a set of expansions - contractions ("sausage mode"). The flapping theory allows both solutions [*Erkaev et al.*, 2009]. In the MHD framework, current sheet flapping may also be induced by BBF propagation within an azimuthally localized flow channel [*Erkaev et al.*, 2009]. In this case, the probe observing flapping (P2) may have been located beside the flow channel and missed the flow. This hypothesis would imply that reconnection took place before 0208 UT, when P2 started observing flapping, and, therefore about 7 min prior to flux transfer onset at P1. This time delay is inconsistent with the tailward velocity observed by P1. Therefore, the scenario implying current sheet instability due to local thinning seems more plausible.

[28] The MHD approach is, however, inadequate to describe thin current sheet dynamics. The current sheet profile reconstruction revealed current sheet thickness comparable to the ion gyroradius and of inertial scale. Kink instability of TCS has been demonstrated in kinetic (PIC and hybrid) simulations [*Pritchett et al.*, 1996; *Karimabadi et al.*, 2003]. PIC simulations of non-Harris current sheet evolution reproduced the sheet surface corrugation with electric current rotation in the *YZ*-plane [*Sitnov et al.*, 2004, 2006]. They also demonstrated temporal changes in TCS thickness during flapping due to a combination of kink and sausage modes. Although the exact mechanism of flapping excitation is not known, its observation for ≈4 min immediately prior to the first reconnection signatures suggests formation of marginally stable TCS. Because only P2 detected current sheet flapping, the TCS was likely localized along *X*, and its length did not exceed 10 R_E.

[29] In addition to being interesting in itself, flapping also makes it possible to scan a portion of plasma sheet and reconstruct vertical profiles of plasma parameters, magnetic field, and its gradient [*Sergeev et al.*, 1998; *Runov et al.*, 2006]. In the context of aforementioned scenario, implying reconnection at $X \approx 15 - 16$ R_E between 0212 and 0213 UT, P2 observations during flapping current sheet crossings provide a unique opportunity to look inside the pre-reconnecting current sheet. Obtained profiles of the vertical magnetic field gradient (a proxy for the cross-tail current density) and electron density (Figures 6 and 7) indicate that a thin current sheet (TCS) was embedded in the thicker current/plasma sheet [*Petrukovich et al.*, 2011]. The TCS scale (half-thickness), ∼100 – 400 km, is comparable to or less than the ion inertial length $d_i = c/\omega_{pi} \approx 400$ km (n = 0.2 cm^{-3}). Profiles reconstructed for three different current sheet crossings exhibit similar structure, indicating the presence of TCS within at least 3 min (0208:50–0211:59 UT). Assuming symmetry with respect to $z = 0$, the profiles suggest fine structural details of the embedded TCS, such as three j_y peaks. A similar structure with a scale of d_i was observed by Cluster near the reconnection region [*Nakamura et al.*, 2006]. Thin current sheets with a sharp peak at the center and secondary peaks at the edges due to electron anisotropy were predicted in analytical models [*Zelenyi et al.*, 2004; *Sitnov et al.*, 2006]. The triple-peak current sheet profile has been also obtained in TCS expansion modeling [*Schindler and Hesse*, 2010].

[30] Another interesting feature observed in reconstructed current density profiles is a local maximum in j_y at the periphery of the current sheet. The electron energy-time spectrogram (Figure 3f) indicates that the high-energy electron flux appeared at $B_X \le -8$ (A+) and $B_X \le -15$ nT (C+, E+). Corresponding electron density profiles (Figure 7) also show some increases at these B_x levels. These observations suggest that local j_y enhancement at the periphery of the current sheet is associated with energetic electron flux enhancement.

[31] Current sheet structure is recognized to be a controlling factor in sheet stability [e.g., *Schindler and Birn*, 1999, 2002; *Schindler*, 2007; *Zelenyi et al.*, 2008]. Thus further theoretical investigation of the formation mechanisms and stability of the observed current sheet structure would be interesting.

[32] Notable features observed in the near-Earth plasma sheet during the interval of interest are positive B_z spikes detected by THEMIS P3 and P4 as well as GOES 10 and 12 and differences in field and particle data observed by P3 and P4. Interpreting the B_z spikes observed by all four spacecraft as signatures of the same dipolarization front, the time delay between the B_z spike detection at THEMIS and GOES probes suggests earthward propagation of the front at 400 km/s, which is consistent with the bulk velocity detected by P4. Magnetic field MVA results (Figure 8a) suggest that the front turns toward midnight meridian during its earthward propagation. The minimum variance direction is typically interpreted as front-normal to the propagating magnetic structure. Assuming that the front has a simple, curved shape and propagates earthward, one can interpret dawnward-directed normal as an indication that the probe is at the dawn-side edge of the front. Accordingly, duskward-directed normal indicates that a probe encounters the front's dusk-side edge [*Sergeev et al.*, 1996; *Nakamura et al.*, 2001]. In our example, the duskward THEMIS probe (P4) detected the front with almost purely earthward-directed normal while P3 observed earthward and dawnward normal. Assuming the simple bubble model [*Sergeev et al.*, 1996], this orientation difference may indicate that P4 was close to the center of the front/bubble and P3 was closer to its dawnward edge. About one minute later, the duskward GOES satellite (G12), detected the front with duskward-directed normal, and the other GOES satellite (G10) observed it with earthward-dawnward normal. Since G12 was located 1.3 R_E dawnward of P4, the normal directions indicate dawnward (toward midnight) deflection of the front/bubble. Similar behavior of a bubble (a flux tube with lower pV^{γ}) and fast flow turning from purely earthward to quasi-radial direction in the premidnight magnetotail was recently shown in MHD simulations with dynamically coupled Lyon-Fedder-Mobarry (LFM) and Rice Convection Model (RCM) [*Pembroke et al.*, 2012; also V. Merkin, private communication, 2011].

[33] The *XZ* projections of MVA front normals at P3 and P4 (Figure 8b) may indicate a curved magnetic field line (flux tube) associated with the front (gray curve). A similar shape has been found in simulations [*Birn et al.*, 2004a] and reported in observations [*Runov et al.*, 2009; *Panov et al.*, 2010; *Li et al.*, 2011].

[34] The plasma velocity vector projections (Figure 8c) show that the pronounced dusk-tailward flow detected by P3 was not observed by P4, located 1.2 R_E earthward and 0.4 R_E duskward of P3. The ion Φ-energy spectrograms (Figure 9e) show clear enhancements in duskward and tailward ion energy fluxes at 1–10 keV and mainly duskward flux enhancement at higher energies. Drift velocity calculations from measured electric and magnetic field result with a duskward velocity of 200 km/s, i.e., smaller duskward velocity than one from ESA and SST measurements. Thus, although the velocity shown in Figure 8c may be overestimated, the duskward flow is well established. The V_y enhancement at P3 persisted for about 2 min. Thus, the plasma involved in traveled a distance of 4 R_E. That it was not captured by P4 implies spatial flow structuring and may indicate vortical plasma motion at dawn-side of the front/BBF. The sense of the vortex is consistent with previous observations [*Keiling et al.*, 2009; *Panov et al.*, 2010] and simulation results [*Birn et al.*, 2011].

[35] Changes in front normal direction and vortex flow pattern in the *XY* plane, observed during front penetration from $X \approx -10$ R_E toward geosynchronous orbit, suggest interchange or ballooning motion of flux tubes in the near-Earth plasma sheet [see, e.g., *Zhu et al.*, 2007, and references therein]. Interchange motion may result in "mushroom"-type structures in fields and plasma pressure [*Guzdar et al.*, 2010; *Birn et al.*, 2011]. A similar structure, called as an "interchange finger head", was recently observed in comprehensive 3-D PIC simulations [see *Pritchett and Coroniti*, 2011, Figure 1c]. Such a structure passing P3 and P4 is shown schematically in Figure 8. (Note that a fragment of MHD simulation results [*Guzdar et al.*, 2010, Figure 3] is out of scale used in Figure 8 for illustration purposes only. The real shape of the head is more complex. We also did not try to scale the clip to fit the observed timing and normal direction.) It is assumed that P4 crossed the "mushroom"-type structure near its center as P3 was hit by its dawn-side wing. This assumption may explain some differences in the P3 and P4 observations in Figures 9 and 10. For example, P4 observed the B_z-enhancement for about a minute, whereas P3 detected only a ~12 s-long spike. For at least one minute, P4 observed a high-energy electron population behind the front; P3 detected only a short (~30 s) enhancement in energetic electron flux (Figures 9g and 10g). Assuming a structure propagation velocity of 300–400 km, a wing thickness of 0.6–0.8 R_E can be estimated. Although the earthward plasma flow at the dipolarization front detected by P4 suggests front formation as a consequence of midtail plasma sheet reconnection, the interchange motion may contribute to steepening of the front [*Pritchett and Coroniti*, 2010; *Hwang et al.*, 2011; *Pritchett and Coroniti*, 2011].

[36] An interesting question is whether the interchange instability developed as a consequence of reconnection or the near-Earth plasma sheet became interchange (ballooning) unstable prior to reconnection in the mid-tail plasma sheet. The timescale of ballooning instability development is ≈600 s [*Zhu et al.*, 2007] or $\approx 40/\Omega_i$, where Ω_i is the ion gyrofrequency [*Pritchett and Coroniti*, 2010]. A relatively thin region with *X*-extent of a few ion gyroradius (approximately 1 R_E) is unstable against kinetic ballooning [*Pritchett and Coroniti*, 2010, 2011]. MHD models suggest that the unstable region extends up to 5 R_E [*Cheng and Zaharia*, 2004; *Raeder et al.*, 2010]. Comparison of B_z time series at P3 and P4 (Figure 1) provides no indication of a local B_z minimum between 0205 and 0215 UT. Thus, development of kinetic interchange (ballooning) instability prior to reconnection is unlikely. On the other hand, if current sheet flapping observed by P2 indicates local thinning of the current sheet at $X \approx -15$ R_E [*Erkaev et al.*, 2009], the ballooning instability criteria may be satisfied there. With the scale of ~5 R_E, obtained in MHD models, one may expect a region near P3/P4 to be unstable. A comparison between B_z at P1 and P2 did not indicate B_z minimum there. Thus, if the B_z minimum was present, it was quite localized in *X* and/or in *Y*. MHD models, however, showed an unstable region with a large azimuthal extent.

[37] Three-dimensional PIC simulations have also shown that azimuthally localized reconnection may develop in the interchange head wake [*Pritchett and Coroniti*, 2011]. Magnetic field, plasma density, and bulk velocity profiles through the head obtained in the simulations are indeed very similar to those observed by P3. Quantitatively, however, the observed B_z peak amplitude is a factor of 2 smaller than the one predicted in the simulations. Moreover, to explain i) the observed small time delay between P4 and P1 observations (~5 s) and ii) signatures of X-line passage underneath of P2, the time delay between initial interchange instability leading to the front formation and subsequent reconnection is required to be much smaller than predicted by the model [*Pritchett and Coroniti*, 2011]. From the observations, we cannot exclude development of interchange independently from reconnection (i.e., absence of causal relationship between signatures detected by P1, P2 and P3/P4). However, the proposed scenario with reconnection at $-15 > X > -16$ R_E is consistent with the observed timing, if the causal relationship is assumed.

[38] A strong earthward electric field component (E_X ~80 mV/m) observed by P4 (Figure 10) indicates ion and electron decoupling due to different gyromotions at the front [*Runov et al.*, 2011]. The appearance of earthward-streaming ions at energies >10 keV ahead of the front, coexisting with the ambient population, is consistent with ion acceleration and reflection at the upcoming front [*Zhou et al.*, 2010]. The P4 observations of electron pitch angle distribution (PAD) with peaks at 0, 180°, and 90° at energies 20–30 keV indicate co-existence of betatron and Fermi-type energization mechanisms at the dipolarization front. Such triple-peak PAD was obtained in test-particle simulations using fields resulting from MHD simulations of magnetotail reconnection [*Birn et al.*, 1997b, 2004b]. The B_z peak value at the front (≈40 nT) was ≈4 times larger than B_z 20–30 s behind it. Thus, the 90°-electron energy of 20–40 keV observed at the B_z peak may result from betatron acceleration of 5–10 keV electrons.

4. Similar Events

[39] The discussed event is not unique. Observations of reconnection at $X \approx -20$ R_E followed by dipolarization front

observations at $X = -10.9$ R_E between 0445 and 0500 UT on 26 February 2008 were reported by *Angelopoulos et al.* [2008]. Reconnection onset time and location were inferred from the time delay between observations at P1 ($X = -21.5$ R_E and P2 ($X = -17.2$ R_E), bracketing the X-line. The earthward-moving dipolarization front was detected182 s later than the inferred reconnection time. This timing suggests a reconnection ejecta propagation velocity of 300–400 km/s, which is generally consistent with the earthward plasma bulk velocity observed at P1 (≈300 km/s) and at P3 (≈500 km/s on average).

[40] In another event (0350–0430 UT, 7 February 2009), reported recently by *Oka et al.* [2011], the most tailward THEMIS probe (P1, $X \approx -30$ R_E) detected a classical flow and field reversal, indicating reconnection onset earthward of P1and tailward X-line retreat. The three inner probes, situated between $X = -9.3$ and -8.3 R_E, detected a distinct earthward-moving dipolarization front about 6 min later. Thus, if reconnection onset was at $-30 < X < -25$ R_E, the timing gives a propagation velocity of 300–400 km/s. The earthward bulk flow velocity, observed by P1 and P2 was, indeed, ≈400 km/s on average.

5. Conclusions

[41] In summary, the presented event study provides evidence of mid-tail magnetic reconnection leading to dipolarization front formation in the near-Earth plasma sheet. This conclusion is in agreement with results from the other event studies.

[42] Although in the discussed case plasma sheet dynamics was triggered mid-tail reconnection, the observations suggest that the interchange instability developed at the reconnection ejecta front during its intrusion into the near-Earth plasma sheet. Interchange or ballooning instability leads to front steepening structuring in the cross-tail direction and to plasma vortex formation aside and behind the front. The question of coupling between reconnection and interchange (ballooning) remains open and requires comprehensive 3D modeling.

[43] Another issue arising from this study is a role of current sheet flapping in the reconnection process. The complex structure of the flapping current sheet observed in the spatial and temporal vicinity of reconnection may signal the instability responsible for reconnection onset. Three-dimensional kinetic modeling and comparison with observations are needed to decode this signal.

[44] Finally, mechanisms of particle energization near dipolarization fronts need to be studied with data analysis and theoretical modeling. Questions regarding the fate of particle intrusion into the near-Earth space along with the dipolarization front should be addressed to future studies including upcoming RBSP measurements. Studies of particle dynamics and energization at the fronts, require multi-point particle measurements with high time resolution. These questions are to be addressed to future space missions such as NASA MMS and JAXA Scope.

[45] **Acknowledgments.** This work was supported by NASA grant NAS5-0299 and NSF grant 1044495. We acknowledge K. H. Glassmeier, U. Auster and W. Baumjohann for the use of FGM data provided under the lead of the Technical University of Braunschweig and with financial support through the German Ministry for Economy and Technology and the German Center for Aviation and Space (DLR) under contract 50 OC 0302; J. W. Bonnell and F. S. Mozer for use of EFI data; C.W. Carlson and J.P. McFadden for use of ESA data; D. Larson and R.P. Lin for use of SST data; A. Roux and O. LeContel for use of SCM data; S. Mende and E. Donovan for use of the ASI data; and the CSA for logistical support in fielding and data retrieval from the GBO stations. GOES data are provided by H.J. Singer. We thank D. Turner, Y. Nishimura and P. Cruce for help with SST and EFI data and software, J. Hohl for help with editing, J. Birn, L. Lyons, V. Merkin, P.L. Pritchett, and M.I. Sitnov, for fruitful discussions.

[46] Masaki Fujimoto thanks the reviewers for their assistance in evaluating this paper.

References

Angelopoulos, V. (2008), The THEMIS mission, *Space Sci. Rev*, *141*, 5–34.

Angelopoulos, V., W. Baumjohann, C. F. Kennel, F. V. Coroniti, M. G. Kivelson, R. Pellat, R. J. Walker, H. Lühr, and G. Paschmann (1992), Bursty bulk flows in the inner central plasma sheet, *J. Geophys. Res.*, *97*, 4027–4039.

Angelopoulos, V., et al. (1994), Statistical characteristics of bursty bulk flow events, *J. Geophys. Res.*, *99*, 21,257–21,280.

Angelopoulos, V., et al. (2008), Tail reconnection triggering substorm onset, *Science*, *321*, 931–935, doi:10.1126/science.1160495.

Angelopoulos, V., et al. (2009), Response to comment on: Tail reconnection triggering substorm onset, *Science*, *324*, 1391, doi:10.1126/science.1168045.

Ashour-Abdalla, M., J.-M. Bosqued, M. El-Alaoui, V. Peroomian, M. Zhou, R. Richard, R. Walker, A. Runov, and V. Angelopoulos (2009), A simulation study of particle energization observed by themis spacecraft during a substorm, *J. Geophys. Res.*, *114*, A09204, doi:10.1029/2009JA014126.

Auster, H. U., et al. (2008), The THEMIS fluxgate magnetometer, *Space Sci. Rev.*, *141*, 235–264.

Baumjohann, W., et al. (2007), Dynamics of thin current sheets: Cluster observations, *Ann. Geophys.*, *25*, 1365–1389.

Birn, J., and E. R. Priest (Eds.) (2007), *Reconnection of Magnetic Fields*, Cambridge Univ. Press, Cambridge, U. K.

Birn, J., M. F. Thomsen, J. E. Borovsky, G. D. Reeves, D. J. McComas, R. D. Belian, and M. Hesse (1997a), Substorm ion injections: Geosynchronous observations and test particle orbits in three-dimensional dynamic mhd fields, *J. Geophys. Res.*, *102*, 2325–2341.

Birn, J., M. F. Thomsen, J. E. Borovsky, G. D. Reeves, D. J. McComas, R. D. Belian, and M. Hesse (1997b), Substorm electron injections: Geosynchronous observations and test particle simulations, *J. Geophys. Res.*, *102*, 2325–2341.

Birn, J., J. Raeder, Y. L. Wang, R. A. Wolf, and M. Hesse (2004a), On the propagation of bubbles in the geomagnetic tail, *Ann.Geophys.*, *22*, 1773–1786.

Birn, J., M. Thomsen, and M. Hesse (2004b), Electron acceleration in the dynamic magnetotail: Test particle orbits in three-dimensional magnetohydrodynamic simulation fields, *Phys. Plasmas*, *11*, 1825, doi:10.1063/1.1704641.

Birn, J., R. Nakamura, E. V. Panov, and M. Hesse (2011), Bursty bulk flows and dipolarization in MHD simulations of magnetotail reconnection, *J. Geophys. Res.*, *116*, A01210, doi:10.1029/2010JA016083.

Bonnell, J. W., F. S. Mozer, G. T. Delory, A. J. Hull, R. E. Ergun, C. M. Cully, V. Angelopoulos, and P. R. Harvey (2008), The electric field instrument (EFI) for THEMIS, *Space Sci. Rev.*, *141*, 303–341.

Cheng, C. Z., and S. Zaharia (2004), MHD ballooning instability in the plasma sheet, *Geophys. Res. Lett.*, *31*, L06809, doi:10.1029/2003GL018823.

Cully, C. M., R. E. Ergun, K. Stevens, A. Nammari, and J. Westfall (2008), The THEMIS digital fields board, *Space Science Rev.*, *141*, 343–355.

Eastwood, J. P., T.-D. Phan, M. Øieroset, and M. A. Shay (2010), Average properties of the magnetic reconnection ion diffusion region in the Earth's magnetotail: The 2001–2005 Cluster observations and comparison with simulations, *J. Geophys. Res.*, *115*, A08215, doi:10.1029/2009JA014962.

El-Alaoui, M., M. Ashour-Abdalla, R. Walker, V. Peroomian, R. L. Richard, V. Angelopoulos, and A. Runov (2009), Substorm evolution as revealed by THEMIS satellites and a global MHD simulation, *J. Geophys. Res.*, *114*, A08221, doi:10.1029/2009JA014133.

Erkaev, N. V., V. S. Semenov, and H. K. Biernat (2008), Magnetic double gradient mechanism for flapping oscillations of a current sheet, *Geophys. Res. Lett.*, *35*, L02111, doi:10.1029/2007GL032277.

Erkaev, N. V., V. S. Semenov, I. V. Kubyshkin, M. V. Kubyshkina, and H. K. Biernat (2009), MHD model of the flapping motions in the magnetotail current sheet, *J. Geophys. Res.*, *114*, A03206, doi:10.1029/2008JA013728.

Ge, Y. S., J. Raeder, V. Angelopoulos, M. L. Gilson, and A. Runov (2011), Interaction of dipolarization fronts within multiple bursty bulk flows in

global MHD simulations of a substorm on 27 February 2009, *J. Geophys. Res.*, *116*, A00I23, doi:10.1029/2010JA015758.
Guzdar, P. N., A. B. Hassam, M. Swisdak, and M. I. Sitnov (2010), A simple MHD model for the formation of multiple dipolarization fronts, *Geophys. Res. Lett.*, *37*, L20102, doi:10.1029/2010GL045017.
Hesse, M., J. Birn, and D. Winske (1998), Formation and structure of thin current sheets in the magnetotail: Dipolarization, in *Substorms 4*, edited by S. Kokubun and Y. Kamide, pp. 727–730, Kluwer Acad., Boston, Mass.
Hwang, K.-J., M. L. Goldstein, E. Lee, and J. S. Pickett (2011), Cluster observations of multiple dipolarization fronts, *J. Geophys. Res.*, *116*, A00I32, doi:10.1029/2010JA015742.
Karimabadi, H., P. L. Pritchett, W. Daughton, and D. Krauss-Varban (2003), Ion-ion kink instability in the magnetotail: 2 Three-dimensional full particle and hybrid simulations and comparison with observations, *J. Geophys. Res.*, *108*(A11), 1401, doi:10.1029/2003JA010109.
Keiling, A., et al. (2009), Substorm current wedge driven by plasma flow vortices: THEMIS observations, *J. Geophys. Res.*, *114*, A00C22, doi:10.1029/2009JA014114.
Krauss-Varban, D., and H. Karimabadi (2003), Timing and localization of reconnection signatures—Is there a substorm model problem?, *Geophys. Res. Lett.*, *30*(6), 1308, doi:10.1029/2002GL016369.
Li, S., V. Angelopoulos, A. Runov, X.-Z. Zhou, J. McFadden, D. Larson, J. Bonnell, and U. Auster (2011), On the force balance around dipolarization fronts within bursty bulk flows, *J. Geophys. Res.*, *116*, A00I35, doi:10.1029/2010JA015884.
Liu, J., C. Gabrielse, V. Angelopoulos, N. A. Frissell, L. R. Lyons, J. P. McFadden, J. Bonnell, and K.-H. Glassmeier (2011), Superposed epoch analysis of magnetotail flux transport during substorms observed by THEMIS, *J. Geophys. Res.*, *116*, A00I29, doi:10.1029/2010JA015886.
McFadden, J. P., C. W. Carlson, D. Larson, V. Angelopolos, M. Ludlam, R. Abiad, and B. Elliot (2008), The THEMIS ESA plasma instrument and in-flight calibration, *Space Sci. Rev.*, *141*, 277–302.
Moore, T., R. Arnoldy, J. Feynman, and D. Hardy (1981), Propagating substorm injection fronts, *J. Geophys. Res.*, *86*, 6713–6726.
Mozer, F. S. (1973), Analysis of techniques for measuring DC and AC electric fields in the magnetosphere, *Space Sci. Rev.*, *14*, 272–313.
Nagai, T., et al. (1998), Structure and dynamics of magnetic reconnection for substorm onsets with Geotail observations, *J. Geophys. Res.*, *103*, 4419–4440.
Nagai, T., M. F. R. Nakamura, W. Baumjohann, W. Ieda, A. Shinohara, S. Machida, Y. Saito, and T. Mukai (2005), Solar wind control of the radial distance of the magnetic reconnection site in the magnetotail, *J. Geophys. Res.*, *110*, A09208, doi:10.1029/2005JA011207.
Nakamura, M. S., H. Matsumoto, and M. Fujimoto (2002a), Interchange instability at the leading part of reconnection jets, *Geophys. Res. Lett.*, *29*(8), 1247, doi:10.1029/2001GL013780.
Nakamura, R., W. Baumjohann, R. Schödel, M. Brittnacher, V. A. Sergeev, M. Kubyshkina, T. Mukai, and K. Liou (2001), Earthward flow bursts, auroral streamers, and small expansions, *J. Geophys. Res.*, *106*, 10,791–10,802.
Nakamura, R., et al. (2002b), Motion of the dipolarization front during a flow burst event observed by Cluster, *Geophys. Res. Lett.*, *29*(20), 1942, doi:10.1029/2002GL015763.
Nakamura, R., et al. (2006), Dynamics of thin current sheets associated with magnetotail reconnection, *J. Geophys. Res.*, *111*, A11206, doi:10.1029/2006JA011706.
Ohtani, S. (1998), Earthward expansion of tail current disruption: Dual-satellite study, *J. Geophys. Res.*, *103*, 6815–6825.
Ohtani, S. I., M. A. Shay, and T. Mukai (2004), Temporal structure of the fast convective flow in the plasma sheet: Comparison between observations and two-fluid simulations, *J. Geophys. Res.*, *109*, A03210, doi:10.1029/2003JA010002.
Oka, M., et al. (2011), Magnetic reconnection X-line retreat associated with dipolarization of the Earth's magnetosphere, *Geophys. Res. Lett.*, *38*, L20105, doi:10.1029/2011GL049350.
Panov, E. V., et al. (2010), Plasma sheet thickness during a bursty bulk flow reversal, *J. Geophys. Res.*, *115*, A05213, doi:10.1029/2009JA014743.
Pembroke, A., F. Toffoletto, S. Sazykin, M. Wiltberger, J. Lyon, V. Merkin, and P. Schmitt (2012), Initial results from a dynamic coupled magnetosphere-ionosphere-ring current model, *J. Geophys. Res.*, *117*, A02211, doi:10.1029/2011JA016979.
Petrukovich, A. A., W. Baumjohann, R. Nakamura, A. Runov, A. Balogh, and H. Rème (2007), Thinning and stretching of the plasma sheet, *J. Geophys. Res.*, *112*, A10213, doi:10.1029/2007JA012349.
Petrukovich, A. A., A. V. Artemyev, H. V. Malova, V. Y. Popov, R. Nakamura, and L. M. Zelenyi (2011), Embedded current sheets in the Earth's magnetotail, *J. Geophys. Res.*, *116*, A00I25, doi:10.1029/2010JA015749.
Pritchett, P. L. (2010), Onset of magnetic reconnection in the presence of a normal magnetic field: Realistic ion to electron mass ratio, *J. Geophys. Res.*, *115*, A10208, doi:10.1029/2010JA015371.
Pritchett, P. L., and F. V. Coroniti (2010), A kinetic ballooning/interchange instability in the magnetotail, *J. Geophys. Res.*, *115*, A06301, doi:10.1029/2009JA014752.
Pritchett, P. L., and F. V. Coroniti (2011), Plasma sheet disruption by interchange-generated flow intrusions, *Geophys. Res. Lett.*, *38*, L10102, doi:10.1029/2011GL047527.
Pritchett, P. L., F. V. Coroniti, and V. K. Decyk (1996), Three-dimensional stability of thin quasi-neutral current sheets, *J. Geophys. Res.*, *101*, 27,413–27,429.
Raeder, J., P. Zhu, Y. Ge, and G. Siscoe (2010), Open Geospace General Circulation Model simulation of a substorm: Axial tail instability and ballooning mode preceding substorm onset, *J. Geophys. Res.*, *115*, A00I16, doi:10.1029/2010JA015876.
Roux, A., O. Le Contel, C. Coillot, A. Bouabdellah, B. de la Porte, D. Alison, S. Ruocco, and M. C. Vassal (2008), The search coil magnetometer for themis, *Space Sci. Rev.*, *141*, 265–275.
Runov, A., et al. (2005a), Electric current and magnetic field geometry in flapping magnetotail current sheets, *Ann. Geophys*, *23*, 1391–1403.
Runov, A., et al. (2005b), Reconstruction of the magnetotail current sheet structure using multi-point Cluster measurements, *Planet. Space Sci.*, *53*, 237–243.
Runov, A., et al. (2006), Local structure of the magnetotail current sheet: 2001 Cluster observations, *Ann. Geophys*, *24*, 247–262.
Runov, A., et al. (2008a), Observations of an active thin current sheet, *J. Geophys. Res.*, *114*, A07S27, doi:10.1029/2007JA012685.
Runov, A., et al. (2008b), Multipoint in situ and ground-based observations during auroral intensifications, *J. Geophys. Res.*, *113*, A00C07, doi:10.1029/2008JA013493.
Runov, A., V. Angelopoulos, M. I. Sitnov, V. A. Sergeev, J. Bonnell, J. P. McFadden, D. Larson, K.-H. Glassmeier, and U. Auster (2009), THEMIS observations of an earthward-propagating dipolarization front, *Geophys. Res. Lett.*, *36*, L14106, doi:10.1029/2009GL038980.
Runov, A., V. Angelopoulos, X.-Z. Zhou, X.-J. Zhang, S. Li, F. Plaschke, and J. Bonnell (2011), A THEMIS multicase study of dipolarization fronts in the magnetotail plasma sheet, *J. Geophys. Res.*, *116*, A05216, doi:10.1029/2010JA016316.
Russell, C. T., and R. L. McPherron (1973), The magnetotail and substorms, *Space Sci. Rev.*, *15*, 205–266.
Saito, M. H., L. N. Hau, C. C. Hung, Y. T. Lai, and Y. C. Chou (2010), Spatial profile of magnetic field in the near-Earth plasma sheet prior to dipolarization by THEMIS: Feature of minimum B, *Geophys. Res. Lett.*, *37*, L08106, doi:10.1029/2010GL042813.
Schindler, K. (2007), *Physics of Space Plasma Activity*, Cambridge Univ. Press, Cambridge, U. K.
Schindler, K., and J. Birn (1999), Thin current sheets and magnetotail dynamics, *J. Geophys. Res.*, *104*, 25,001–25,010.
Schindler, K., and J. Birn (2002), Thin current sheets in the magnetotail and the loss of equilibrium, *J. Geophys. Res.*, *107*(A7), 1117, doi:10.1029/2001JA000291.
Schindler, K., and M. Hesse (2010), Conditions for the formation of non-gyrotropic current sheets in slowly evolving plasmas, *Phys. Plasmas*, *17*, 082103, doi:10.1063/1.3464198.
Schödel, R., W. Baumjohann, R. Nakamura, V. A. Sergeev, and T. Mukai (2001a), Rapid flux transport in the central plasma sheet, *J. Geophys. Res.*, *106*, 301–313.
Schödel, R., R. Nakamura, W. Baumjohann, and T. Mukai (2001b), Rapid flux transport and plasma sheet reconfiguration, *J. Geophys. Res.*, *106*, 8381–8390.
Semenov, V. S., I. V. Kubyshkin, V. V. Lebedeva, R. P. Rijnbeek, M. F. Heyn, H. K. Biernat, and C. J. Farrugia (1992), A comparison and review of steady-state and time-varying reconnection, *Planet. Space Sci.*, *40*, 63–87.
Sergeev, V., T. I. Pulkkinen, R. J. Pellinen, and N. A. Tsyganenko (1994), Hybrid state of the tail magnetic configuration during steady convection events, *J. Geophys. Res.*, *99*, 23,571–23,582.
Sergeev, V. A., V. Angelopoulos, J. T. Gosling, C. A. Cattell, and C. T. Russell (1996), Detection of localized, plasma-depleted flux tubes or bubbles in the midtail plasma sheet, *J. Geophys. Res*, *101*, 10,817–10,826.
Sergeev, V., V. Angelopoulos, C. Carlson, and P. Sutcliffe (1998), Current sheet measurements within a flapping plasma sheet, *J. Geophys. Res*, *103*, 9177–9188.
Sergeev, V., et al. (2003), Current sheet flapping motion and structure observed by Cluster, *Geophys. Res. Lett.*, *30*(6), 1327, doi:10.1029/2002GL016500.
Sergeev, V., A. Runov, W. Baumjohann, R. Nakamura, T. L. Zhang, A. Balogh, P. Louarn, J.-A. Sauvaud, and H. Rème (2004), Orientation

and propagation of current sheet oscillations, *Geophys. Res. Lett.*, *31*, L05807, doi:10.1029/2003GL019346.

Sergeev, V. A., D. A. Sormakov, S. V. Apatenkov, W. Baumjohann, R. Nakamura, A. Runov, T. Mukai, and T. Nagai (2006), Survey of large-amplitude flapping motions in the midtail current sheet, *Ann. Geophys.*, *24*, 2015–2024.

Sergeev, V., et al. (2008), Study of near-earth reconnection events with Cluster and Double Star, *J. Geophys. Res.*, *113*, A07S36, doi:10.1029/2007JA012902.

Sergeev, V., V. Angelopoulos, S. Apatenkov, J. Bonnell, R. Ergun, J. McFadden, D. Larson, R. Nakamura, and A. Runov (2009), Structure of injection front in the flow braking region, *Geophys. Res. Lett.*, *36*, L21105, doi:10.1029/2009GL040658.

Sibeck, D. G., and V. Angelopoulos (2008), THEMIS science objectives and mission phases, *Space Sci. Rev.*, *141*, 35–59.

Sitnov, M. I., and K. Schindler (2010), Tearing stability of a multiscale magnetotail current sheet, *Geophys. Res. Lett.*, *37*, L08102, doi:10.1029/2010GL042961.

Sitnov, M. I., and M. Swisdak (2011), Onset of collisionless magnetic reconnection in two-dimensional current sheets and formation of dipolarization fronts, *J. Geophys. Res.*, *116*, A12216, doi:10.1029/2011JA016920.

Sitnov, M. I., M. Swisdak, J. F. Drake, P. N. Guzdar, and B. N. Rogers (2004), A model of the bifurcated current sheet: 2. Flapping motion, *Geophys. Res. Lett.*, *31*, L09805, doi:10.1029/2004GL019473.

Sitnov, M. I., M. Swisdak, P. N. Guzdar, and A. Runov (2006), Structure and dynamics of a new class of thin current sheets, *J. Geophys. Res.*, *111*, A08204, doi:10.1029/2005JA011517.

Sitnov, M. I., M. Swisdak, and A. V. Divin (2009), Dipolarization fronts as a signature of transient reconnection in the magnetotail, *J. Geophys. Res.*, *114*, A04202, doi:10.1029/2008JA013980.

Sonnerup, B. U. Ö., and M. Scheible (1998), Minimum and maximum variance analysis, in *Analysis Methods for Multi-spacecraft Data*, *ISSI Sci. Rep. Ser.*, vol. 1, edited by G. Paschmann and P. Daly, pp. 185–220, Eur. Space Agency, Noordwijk, Netherlands.

Tsyganenko, N. A. (1995), Modeling the Earth's magnetospheric magnetic field confined within a realistic magnetopause, *J. Geophys. Res.*, *100*, 5599–5612.

Vasyliunas, V. M. (1975), Theoretical models of magnetic field line merging. I., *Rev. Geophys.*, *13*, 303–336.

Wiltberger, M., T. I. Pulkkinen, J. G. Lyon, and C. C. Goodrich (2000), MHD simulation of the magnetotail during the December 10, 1996, substorm, *J. Geophys. Res.*, *105*, 27,649–27,663.

Zelenyi, L. M., H. V. Malova, V. Y. Popov, D. Delcourt, and A. S. Sharma (2004), Nonlinear equilibrium structure of thin current sheets: Influence of electron pressure anisotropy, *Nonlinear Processes Geophys.*, *11*, 579–587.

Zelenyi, L., A. Artemiev, H. Malova, and V. Popov (2008), Marginal stability of thin current sheets in the Earth's magnetotail, *J. Atmos. Sol. Terr. Phys.*, *70*, 325–333.

Zhang, X.-J., V. Angelopoulos, A. Runov, X.-Z. Zhou, J. Bonnell, J. P. McFadden, D. Larson, and U. Auster (2011), Current-carriers near dipolarization fronts in the magnetotail: A THEMIS event study, *J. Geophys. Res.*, *116*, A00I20, doi:10.1029/2010JA015885.

Zhou, X.-Z., V. Angelopoulos, A. Runov, M. I. Sitnov, Q.-G. Zong, and Z. Y. Pu (2009), Ion distributions near the reconnection sites: Comparison between simulations and THEMIS observations, *J. Geophys. Res.*, *114*, A12211, doi:10.1029/2009JA014614.

Zhou, X.-Z., V. Angelopoulos, V. A. Sergeev, and A. Runov (2010), Accelerated ions ahead of earthward-propagating dipolarization fronts, *J. Geophys. Res.*, *115*, A00I03, doi:10.1029/2010JA015481.

Zhou, X.-Z., V. Angelopoulos, V. A. Sergeev, and A. Runov (2011), On the nature of precursor flows upstream of advancing of dipolarization fronts, *J. Geophys. Res.*, *116*, A03222, doi:10.1029/2010JA016165.

Zhu, P., C. R. Sovinec, C. C. Hegna, A. Bhattacharjee, and K. Germaschewski (2007), Nonlinear ballooning instability in the near-Earth magnetotail: Growth, structure, and possible role in substorms, *J. Geophys. Res.*, *112*, A06222, doi:10.1029/2006JA011991.